Dynamic Power Control In Utility-Connected Microgrids: A Back To Back Converter Approach For Efficient Integration Of Solar And Wind Energy

L. Nadam[1] , Dr.M. Chakravarthy[2] , Dr.M. Manjula[3]

[1]Research Scholar Osmania University-Hyderabad
lavudyanadam@gmail.com

[2]Professor Vasavi college of Engg-Hyd
muktevichakri@gmail.com

[3]Professor University College of Engg Osmania University-Hyd.

Abstract: -

This research directs the imperative need for robust power management and control in utility-connected microgrids featuring solar and wind energy sources. The suggested method employs back to back converters for precise control on the transfer of both active and reactive power between the microgrid and the utility. The new control strategy operates in two states, effectively sharing power among the utility and the microgrid. An innovative arrangement among DGs ensures seamless load sharing in both grid-connected (GCM) and islanded modes (IM). The back-to-back converters provide complete frequency isolation, protecting the microgrid from voltage or frequency fluctuations from the utility side. The study introduces synchronized relay-breaker operation during faults, along with disabling back to back converters, ensuring smooth resynchronization after fault clearance. System stability is confirmed under different load changes. The proposed control setup proves resilient to changes in grid-side voltage and frequency, ensuring a stable and reliable power-sharing mechanism under various operating conditions. Simulations conducted in MATLAB/SIMULINK validate the efficacy of the proposed control strategy, highlighting its ability to enhance the stability and reliability of utility-connected microgrids incorporating solar and wind energy sources. This study contributes to advancing sustainable energy solutions, advocating for resilient and eco-friendly power systems.

Keyword: Active power, Reactive power, Back-to-Back converter, Microgrid and Utility grid

1. Introduction

Over the last few decades, numerous substantial blackouts have been documented in electric power networks worldwide, leading to significant economic losses in the respective regions [1-2]. Faults in power systems have various origins, spanning from localized issues initiated by transmission line failures and technical problems at power plants to widespread faults arising from unfavourable weather conditions or natural disasters. These incidents raise significant concerns, especially as essential facilities like hospitals, airports, and continuous process industries often experience prolonged disruptions, lasting from 5 to 10 hours and sometimes even longer. Additionally, the restoration of the grid often requires a significant amount of time after extensive blackouts. In some cases, even operational transmission lines may require temporary deactivation to facilitate the restoration of the grid [3]. As a result, addressing concerns about the future of power grids worldwide becomes an urgent necessity. An example of this rearrangement is the implementation of MGs, deployed in moderately insignificant topographical areas and coupled on the distribution system. MGs may operate in both GCM and IM modes. This versatility makes them well-suited for deployment in isolated areas, such as countryside zones, efficiently excluding the requirement for costly infrastructure [4]. Additionally, MG may independently disconnect from the main grid during power failure or adjacent faults. This enhances the reliability and resilience of local systems, especially important for sensitive consumers during environmental calamities.

However, a malfunction in any renewable source might significantly impact the entire system, particularly if Energy Storage Systems (ESS) are not well-employed. MGs require sophisticated power regulation schemes to ensure the efficient working and regulation of renewable sources to reach stability and other microgrid requirements. The improvement of power regulation for MGs has garnered significant concentration in the recent years, covering a range of proposed concepts, from numerical methods to novel optimization techniques.

Furthermore, optimization techniques are widely used to optimize the dispatch of renewable sources for minimizing total running expenses. A literature survey on this reveal that quite a lot of research have been undertaken in this domain. The power regulation for MGs, particularly in buildings, focuses on handling thermal energy and power distribution. In [6] concentrated on power regulation and controlling of MGs. In [7], authors evaluated power regulation for DC Microgrids. In [8] covered a wider range of optimization methods, and Al-Ismail [9] critically analyses EMCS methods. Classification of power management systems of microgrids is discussed in [10].

In [11], authors suggest a separate control plan for batteries and supercapacitors, using a Type II controller for one and a nonlinear PI controller for the other. The goal is to keep bus voltage and power quality stable during abrupt changes in power in a low-voltage DC microgrid. In [12], they introduce a secondary voltage control system in a DC microgrid to reduce sudden voltage changes caused by decentralized local power controllers in DERs. In [13], they suggest a control system for DC microgrids, where an AC voltage signal is added to the DC voltage of the microgrid, enhancing voltage regulation.

In [14], Authors propose integrating a nonlinear adaptive controller with MPPT to control the DC bus voltage during islanded operation and grid transitions in a microgrid. The importance is on selecting MPPT control to optimize the utilization of RES. Additionally, the adaptive parameters of the droop controller are optimized using sequential quadratic programming. In [15], an FOPID controller is used to control the DC bus voltage in a hybrid microgrid designed for remote and islanded operation. In [16], an implemented control system relies on a normalized gradient adaptive regularization factor neural filter for an AC microgrid powered by a PV-BESS. The primary objective of this control strategy is to regulate the DC link voltage of the voltage source converter, ensuring optimal power extraction from the PV source.

In [17], a voltage control system is proposed as part of the secondary control stage within a distributed multi-agent system structure. This system is designed to regulate both voltage and frequency, correcting Voltage-Frequency (V-F) deviations caused by the droop controller in the primary control stage. In [18] introduced an adaptive droop-based cooperative scheme to distribute the load among BESS installed in a PV-BESS based DC microgrid. In [19] utilized a

virtual impedance-based droop control to share the load among parallel voltage source inverters without the need for communication to coordinate power sharing. In [20] presented an adaptive power-sharing approach for FC and generic ESS within DC microgrids, employing the k-sharing method known for its high stability levels and minimal disruptions at the FC terminals. In [21] introduced a fuzzy adaptive compensation control to correct disproportionate reactive power sharing caused by mismatched impedances in distributed generation. The controller achieves this by dynamically adjusting the voltage reference signal of the DERs in real-time. In [22], the study focused on superimposed frequency droop control for power sharing in DC microgrids, introducing two parameters to enhance stability and address loading issues: the adaptive voltage coupling gain and adaptive amplitude of the injected AC voltage. The control of these parameters improves system operation under changing loading conditions.

The principal goal of this paper is to develop a microgrid incorporating distributed generators using power electronics. Solar and wind generation systems serve as DGs connected to the grid through back-to-back converters, facilitating bidirectional power flow control between the utility and the microgrid. The back-to-back converters are pivotal in maintaining essential frequency and power quality isolation, thereby enhancing the overall reliability and resilience of the microgrid. The proposed setup underscores the importance of controlled and coordinated power electronics interfacing in distributed generation systems. The objectives of the paper are outlined as follows:

- Investigate the use of back to back converters for power flow regulation in grid-connected DGs, with a focus on their role in facilitating bidirectional power transfer between the MG and the grid.
- Design of a dynamic control with two states for efficient sharing of active and reactive power between the grid and the MG, adapting to the power requirements of the consumers.
- Investigate innovative configurations of renewable sources within the microgrid to improve load-sharing in Grid-Connected Mode (GCM) and Islanded Mode (ISM), fostering resilience and optimizing resource utilization.

- Evaluate the complete frequency isolation achieved by the back-to-back converters, ensuring that voltage or frequency variations in the utility grid do not impact the microgrid, thereby preserving stability.
- Validate the proposed control strategy through comprehensive simulation studies using the MATLAB/SIMULINLK tool, considering diverse load types, fault scenarios, and unexpected events such as fluctuations in DC side voltage and DG tripping.

2. Structure of the system

A single line diagram of the adopted system with grid, PV and wind generation systems and interconnected back to back converters are shown in Figure 1. VSC-1 and VSC-2 are two voltage source converters connected in back to back configuration for power exchange between PVGS, WGS and grid. Both these converters draw power from a DC link capacitor with a voltage denoted as $\mathrm{V_c}$. Both the PVGS and WGS are linked to the microgrid using another two voltage source converters VSC-3 and VSC-4.

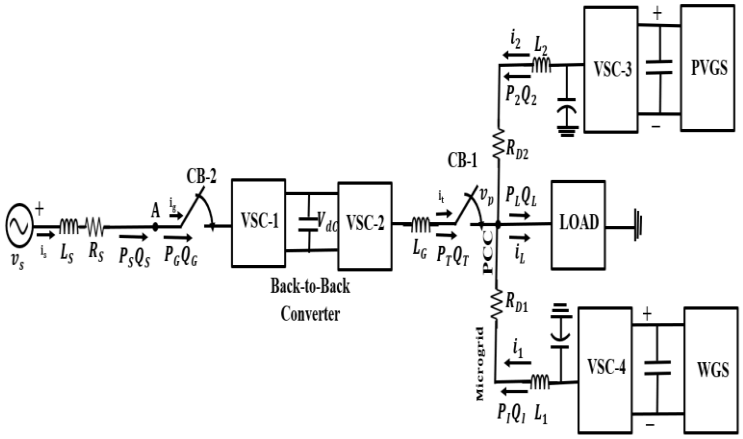

Figure 1. System Structure

The DGs' output inductances are termed as $\mathrm{L_1}$ and $\mathrm{L_2}$. $\mathrm{P_1Q_1}, \mathrm{P_2Q_2}$ and $\mathrm{P_LQ_L}$ are the real and imaginary powers at the terminals of WGS, PVGS and load respectively. Grid voltage is termed $\mathrm{V_S}$. $\mathrm{R_S}$ and $\mathrm{L_S}$ are grid resistance and inductance respectively. $\mathrm{R_{D1}}, \mathrm{L_1}$ and $\mathrm{R_{D2}}, \mathrm{L_2}$ are the line resistance and inductances of WGS and PVGS respectively. CB1 and CB2 are the circuit breakers which connects or disconnects grid to the renewable sources. $\mathrm{P_T}$, $\mathrm{Q_T}$ are the active and reactive power supplied from grid to the microgrid. The system can operate in two states based on the microgrid's power requirements. In State 1, a reference amount of real and reactive power which

are given to control system of the back to back converter are provided by the grid to the load. Remaining power required by the load can be provided by the PVGS and WGS in proportional to their ratings. If the power demand in the microgrid exceeds the total generation capacity of both PVGS and WGS due to atmospheric disturbances state 1 is not feasible. Hence in those conditions, using State-2 control, the grid will provide the additional power required, while the DGs operate at their peak capacity.

When both DGs generate respective peak power, the MG shifts from State-1 to State-2. Though State-1 ensures a predefined power flow from the grid, State-2 offers a more consistent regulation of the back to back converter and can control significant uncertainties in both consumer side and generation side. The maximum capacity of the back to back converters depends on the peak value of the power that should be transferred through it. The peak power flow takes place when the MG experiences its highest load demand, and the DGs generate the minimum power. As a result, power flows from the grid to the microgrid. Moreover, when the DGs produce maximum power while the load demand in the microgrid is at its minimum, it results in power flowing from the MG to the grid. The rating concern needs to be predetermined, ensuring that the MG cannot provide or allow further power than the required limit.

3. Converters Control Strategy

VSC-3 converter is comprising of 3 H-bridges and three Y connected 1-ϕ transformers and DC side is connected to the PVGS as presented in figure 2. The resistance R_f is included to consider switching and transformer losses. To mitigate switching harmonics, an LCL filter is selected. VSC-4 for WGS adopts a 6-pulse universal bridge as a converter. The converters of the back to back configuration share the same 2 universal bridges, interconnected through a DC link capacitor with a voltage of V_C as illustrated in Figure 1.

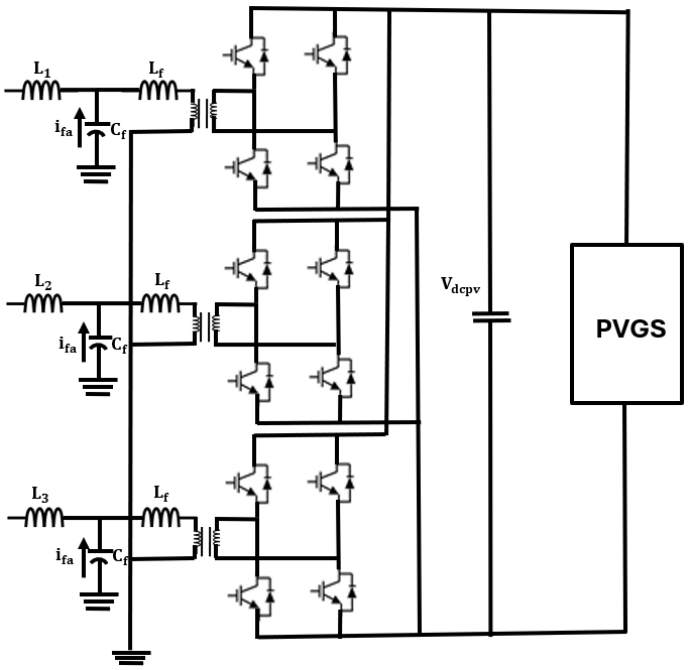

Figure 2. Converter Structure of VSC-3

The control strategy governs all four VSCs. Each of these controllers requires its own set of instantaneous reference voltages for generating switching pulses by SPWM.

3.1. Reference signal Generation for VSC-1

The controller angle required by VSC-1 is produced as depicted in Figure 3. Initially, the measured capacitor voltage goes through low-pass filtering, followed by a comparison with the reference DC link voltage $\mathrm{V}_{\mathrm{dc}}^{\mathrm{ref}}$. The resulting difference between actual and reference voltage is then processed by a PI regulator to produce the reference angle δ_{ref}. Consequently, the instantaneous reference voltages of the three phases are determined using controller reference angle δ_{ref} and voltage peak value of 1.

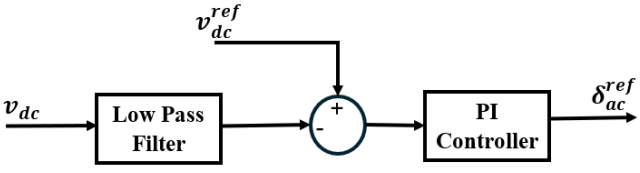

Figure 3. Reference angle generation for VSC-1

3.2. Reference signal generation for VSC-2 in State-1

In State-1, P_{ref} and Q_{ref} are the required active and reactive powers which should be transferred between grid and MG through VSC-2. The output voltage of VSC-2 is represented by

$V_T\angle\delta_T$, and the PCC voltage is denoted by $V_P\angle\delta_P$. Then the reference voltage magnitude and angle at the terminals of VSC-2 can be defined as:

$$V_T^{ref} = \frac{V_P^2 + Q_{ref}X_G}{V_P COS(\delta_T - \delta_P)} \#(1)$$

$$\delta_T^{ref} = tan^{-1}\left(\frac{P_{ref}X_G}{V_P^2 + Q_{ref}X_G}\right) + \delta_P \#(2)$$

These references are computed subject to the load demand. Reference voltage can be calculated by using V_T^{ref} and δ_T^{ref}. And switching pulses are generated by SPWM. The sign of the reference active and reactive powers should be negative if power transfer is from MG to the grid.

3.3. Reference signal generation for VSC-2 in State-2

In State 2, if both DGs supply their maximum available power, the grid compensates for any power shortage of consumers by utilizing the back-to-back converters. Let P_{max} and Q_{max} denote the peak capacity of the back to back converters. Then reference voltage magnitude and controller angle are calculated as follows:

$$\delta_T = \delta_{max} - m_T \times (P_T - P_{max}) \#(3)$$

$$V_T = V_{max} - n_T \times (Q_T - Q_{max}) \#(4)$$

Here, V_{max} and δ_{max}represent the magnitude and controller angle of the reference voltage, when supplying the maximum load. m_T and n_T are the droop coefficients and can be chosen depending on power limits of the converter.

3.4. Signal generation for VSC-3 in State-1

In State 1, it is considered that the grid provides a fraction of the consumers requirement, and both DGs supply and regulate the remaining requirement of the consumer. The converted voltages by VSC-3 can be controlled by considering the load proportionally of its respective DG. Controlling the real and reactive power from PVGS to the microgrid involves adjusting the magnitude and controller angle of the voltage. Injected active and reactive powers from the PVGS is given as

$$P_1 = \frac{V_1 \times V_{P1} sin(\delta_1 - \delta_{P1})}{X_1} \#(5)$$

$$Q_1 = \frac{V_1^2 - V_1 \times V_{P1} cos(\delta_1 - \delta_{P1})}{X_1} \#(6)$$

if the difference between phase angle of V_1 and phase angle of V_{p1} is less then the active power provided by PVGS may be regulated by δ_1 and reactive power can be regulated by V_1. This enables the distribution of power requirements among the DGs, by adjusting the V_1 and δ_1 using droop coefficients which is given as follows:

$$\delta_1 = \delta_{1rated} - m_1 \times (P_1 - P_{1rated}) \#(7)$$

$$V_1 = V_{1rated} - n_1 \times (Q_1 - Q_{1rated}) \#(8)$$

In this equation, δ_{1rated} and V_{1rated} denote the rated magnitude and angle of the voltage of PVGS when it is delivering P_{1rated} and Q_{1rated} power to the load. m_1 and n_1 are the droop coefficients for controller angle to regulate active power and for magnitude to regulate reactive power respectively. As both DGs are converter-based, enabling instantaneous changes in the controller angle, the angle droop facilitates load sharing lacking any reduction in fundamental frequency. In a microgrid featuring frequency droop, the angular shift associated with regular load fluctuations tends to be more significant than the changes observed in the overall system fundamental frequency. If this issue is addressed with a low droop coefficient, it might result in significant frequency variations. Angle droop helps mitigate this frequency variation to some extent.

$$\delta_1 - \delta = (X_1 + X_{L1})P_1 \#(9)$$

$$\delta_2 - \delta = (X_2 + X_{L2})P_2 \#(10)$$

Where

$$X_1 = \frac{\omega L_1}{(VV_1)},\ X_2 = \frac{\omega L_2}{(VV_2)},\ X_{L1} = \frac{\omega L_{Line1}}{(VV_1)},\ X_{L2} = \frac{\omega L_{Line2}}{(VV_2)}\ \#(11)$$

The angle droop equation of the DGs is

$$\delta_1 = \delta_{1rated} - m_1 \times (P_1 - P_{1rated}) \#(12)$$

$$\delta_2 = \delta_{2rated} - m_2 \times (P_2 - P_{2rated}) \#(13)$$

$\delta_{1rated} = m_1 P_{1rated}$ and $\delta_{2rated} = m_2 P_{2rated}$

Then

$$\delta_1 - \delta_2 = m_1 P_1 - m_2 P_2 \#(14)$$

Similarly

$$\delta_1 - \delta_2 = (X_1 + X_{L1})P_1 - (X_2 + X_{L2})P_2 \#(15)$$

Assuming a lossless system, we obtain:

$$(X_1 + X_{L1})P_1 - (X_2 + X_{L2})(P_L - P_1) = m_1 P_1 - m_2 (P_L - P_1) \#(16)$$

$$P_1 = \frac{X_2 + X_{L2} + m_2}{X_2 + X_{L2} + m_2 + X_1 + X_{L1} + m_1} P_L \#(17)$$

Similarly, P_2 can be determined as

$$P_2 = \frac{X_1 + X_{L1} + m_1}{X_2 + X_{L2} + m_2 + X_1 + X_{L1} + m_1} P_L \#(18)$$

the output power ratio is calculated as:

$$\frac{P_1}{P_2} = \frac{X_2 + X_{L2} + m_2}{X_1 + X_{L1} + m_1} \#(19)$$

It is significant that the values of X_1 and $X_2$are considerably smaller compared to the values of m_1 and m_2. Moreover, considering the predominantly resistive nature of the microgrid line with minimal inductance and the significantly larger inductance

$$m_1 \gg X_1 \gg X_{L1} \; and \; m_2 \gg X_2 \gg X_{L2} \#(20)$$

the droop coefficients can be expressed as:

$$\frac{P_1}{P_2} \approx \frac{m_2}{m_1} = \frac{P_{1rated}}{P_{2rated}} \#(21)$$

A high droop coefficient will consistently exert a significant impact, ensuring efficient power sharing with minimal deviation. Reactive power sharing has traditionally relied on the drop in voltage magnitude. As the converter output impedance is inductive, alterations in the controller angle have a minimal impact on sharing of imaginary power.

Therefore, PVGS can provide the required power if the terminal voltage of VSC-3 maintains the specified magnitude and angle as described in equation (5 and 6). The same approach can generate the require refence signals by VSC-4 to generate the switching pulses using SPWM

3.5. Signal generation for VSC-3 in State-2

In state 2, the PV and wind systems generate their permissible peak power and remaining required power by the load can be provided by the grid. Using required active power and reactive power termed as P_{1avail} and Q_{1avail} reference voltage magnitude and controller angle can be calculated as:

$$V_1 = \frac{{V_{P1}}^2 + Q_{1avail} X_1}{V_{P1} cos(\delta_{P1} - \delta_P)} \#(22)$$

$$\delta_1 = \left(\frac{P_{1avail}\, X_1}{{V_{P1}}^2 + Q_{1avail}\, X_1}\right) + \delta_{P1} \#(23)$$

4. Distributed Generation

4.1. PV Generation system

Equivalent circuit for a PV cell includes basic components, as shown in Fig. 4.

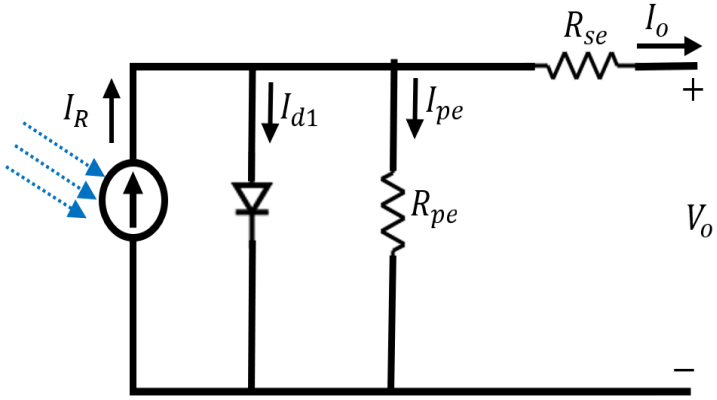

Figure. 4. Equivalent circuit of PV cell

Output current of the PV cell can be calculated as

$$i_o = I_R - I_{d1} - I_{pe} \#(24)$$

$$i_{d1} = I_{01}\left(e^{q\frac{(v_{pv}+i_{pv}R_{se})}{nKT}}\right) - 1 \#(25)$$

Equation (26) shows the fundamental expression for the current made by a PV cell.

$$I_R = \frac{W}{W_0}\left(I_C + \lambda(T - T_0)\right) \#(26)$$

$$i_{pv} = I_R - I_{01}\left[\left(e^{q\frac{(v_{pv}+i_{pv}R_{se})}{nKT}}\right) - 1\right] - \frac{(v_{pv}+i_{pv}R_{se})}{R_{Pe}} \#(27)$$

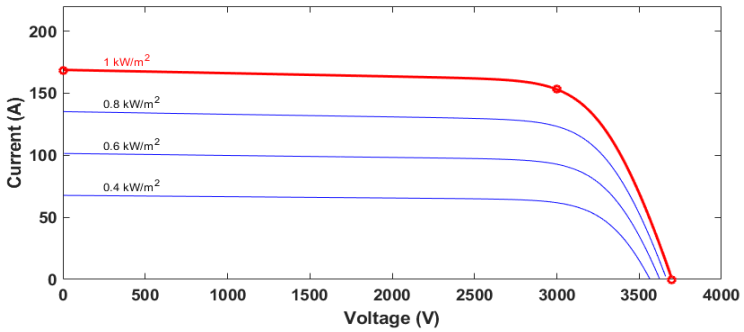

(a)

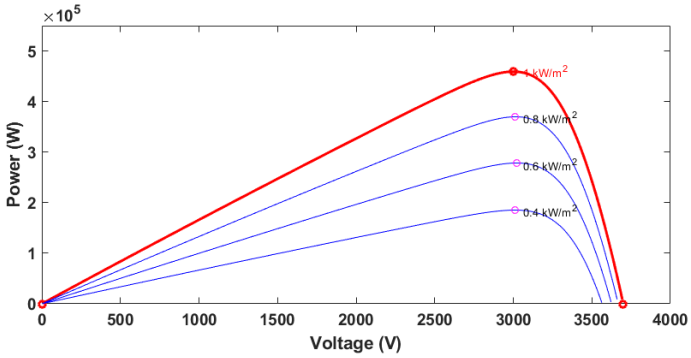

(b)

Fig. 5. VI and PI Characteristics of PV array

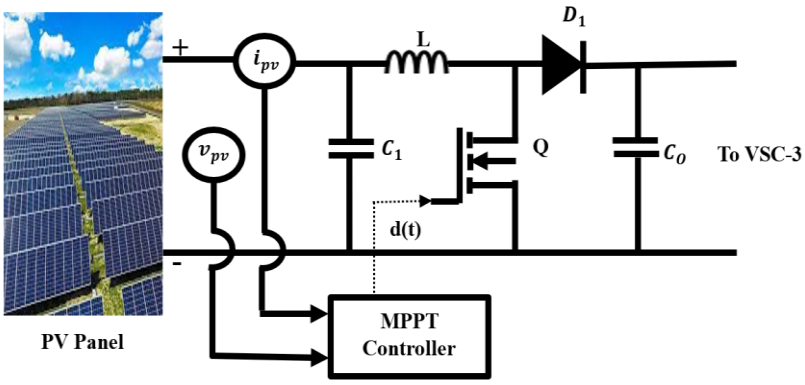

Figure.6. PV Generation system

The I_{01} is defined by:

$$I_{01} = I_{01ref}\left(\frac{T}{T_O}\right)^3 e^{\left[\frac{qE_G}{nK}\left(\frac{1}{T}-\frac{1}{T_O}\right)\right]} \#(28)$$

where E_G is the energy bandgap.

To fulfil the basic power requirements, solar cells, which generate relatively low power, can be linked in series to create panels. These panels, in turn, can be connected in either parallel or series configurations to construct PV arrays. As presented in Fig. 5, the MPP changes with atmospheric conditions, requiring the use of a maximum power tracking algorithm to align the PV output power nearer to the maximum power point. From the characteristics shown in fig 5(b) the maximum power point is achieved when $\frac{dp}{dv} = 0$. The Adaptive MPPT controller required by PVGS is designed by the relation given as.

$$\frac{dp}{dv_{pv}} = \begin{cases} = 0, \ at\ MPP \\ > 0, at\ side\ of\ MPP \\ < 0, at\ right\ side\ of\ MPP \end{cases} \quad \#(29)$$

4.2. Wind Generation system

The model of wind power is

$$P_{wind} = \frac{1}{2} \times \rho \times s \times v_{\omega}^{3} \#(30)$$

$$P_{turb} = C_p(A,\beta) \times P_{wind} = \frac{1}{2} \times \rho \times s \times C_p(A,\beta) \times v_{\omega}^{3} \#(31)$$

$$T_{turb} = \frac{P_{turb}}{\Omega_t} = \frac{1}{2} \times \varphi \times s \times C_p(A,\beta) \times v_{\omega}^{3} \times \frac{1}{\Omega_t} \#(32)$$

where C_p is a power coefficient adopted to the wind turbine

$$\begin{cases} C_p(A,\beta) = 0.5176\left(\frac{116}{A} - 0.4\beta - 4\right) + 0.0068 \times \lambda \times e^{\frac{-21}{A}} \\ \frac{1}{\lambda} = \frac{1}{\lambda + 0.08.\beta} - \frac{0.035}{1+\beta^3} \\ \lambda = \frac{\Omega_t \times R}{V_{\omega}} \\ C_p^{max}(\lambda,\beta) = \frac{16}{27} = 0.5930 \end{cases} \#(33)$$

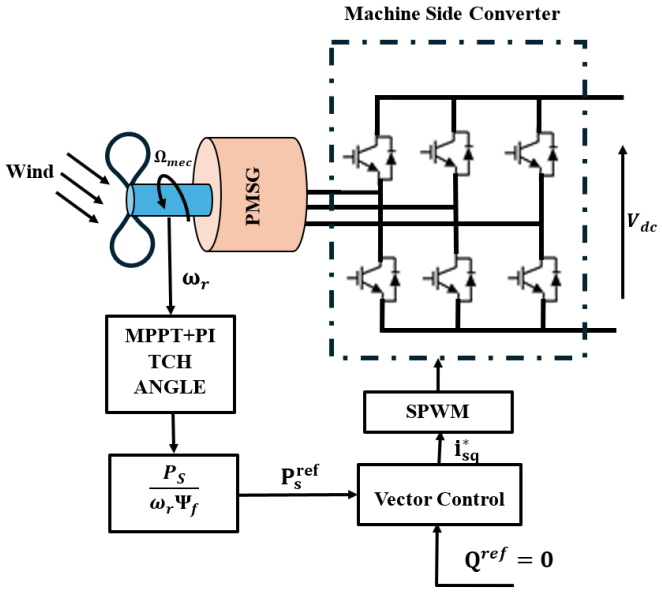

Figure 7. PMSG based wind generation system (WGS)

4.3. Machine-side converter control (MSC)

Stator voltage equations of wind connected PMSG is given as

$$\begin{cases} U_{sd} = R_s i_{sd} + L_{sd}\frac{di_{sd}}{dt} - \omega_r L_{sq} i_{sq} \\ U_{sq} = R_s i_{sq} + L_{sq}\frac{di_{sd}}{dt} + \omega_r L_{sq} i_{sq} + \omega_r \Psi_f \end{cases} \#(34)$$

The terms "U_{sd}" and "U_{sq}" denote the stator voltage direct and quadrature axis components, respectively. The parameter

"R_s" represents the stator resistance, while i_{sd}" and "i_{sq}" denote the stator direct and quadrature currents. Additionally, "L_{sd}" and "L_{sq}" refer to the stator direct and quadrature axis inductances.

The MSC employs a control strategy that prioritizes the maintenance of zero d-axis current. This approach depends on the orientation of the rotor magnetic flux and is designed to keep the rotor current, denoted as i_{sd} consistently at zero.

$$\begin{cases} P_s = -\dfrac{3}{2}U_{sq}i_{sq} \\ Q_s = -\dfrac{3}{2}U_{sd}i_{sq} \\ T_e = -\dfrac{3}{2}P_n i_{sq}\Psi_f \end{cases} \#(35)$$

The P_s and Q_s represent the stator active and reactive powers, respectively. In steady state, the differentials of i_{sd} and i_{sq} are both zero. The inner-loop current regulation utilizes PI control in vector control. Consequently, the dynamic equation for the PMSG can be obtained from Equation (34) is given as.

$$\begin{cases} U_{sd} = R_s i_{sd} - \omega_r L_{sq} i_{sq} + \left(K_P + \dfrac{K_1}{S}\right)(i_{sd}^* - i_{sd}) \\ U_{sq} = R_s i_{sq} + \left(K_P + \dfrac{K_1}{S}\right)(i_{sq}^* - i_{sq}) + \omega_r L_{sd} i_{sd} + \omega_r \Psi_f \end{cases} \#(36)$$

The gains for the current inner loop adjustments are denoted by K_P and $K_I$respectively. The reference values for the stator currents i_d and i_q are denoted as $i_{sd}^*$and i_{sq}^* respectively.

Figure 8 illustrates the control block diagram for the machine-side converter of the PMSG wind turbine. This control strategy utilizes a double feedback control configuration. The external PI control loop regulate DC voltage, and its output is used as reference for the quadrature current required by the inner loop. In the inner PI control loop, reference direct axis current is adopted as 0 for improved power factor. The control scheme includes current decoupling, as expressed in Equation (16), enabling unrestricted derivative tracking of the current.

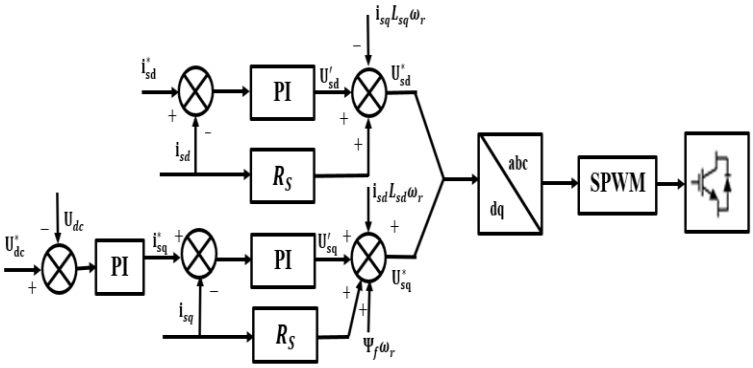

Figure 8. Machine Side Converter Control System

5. Simulation Results

Simulation studies are conducted in MATLAB/SIMULINK considering various load configurations and load-sharing scenarios. The DGs are modelled as wind and PV generation systems. Table I presents the system data. Load changes, frequency variations, and voltage disturbances at the grid side are taken into account to assess the effectiveness of the proposed strategy.

Table 1. System Parameters

Parameters	**Values**
Grid Voltage and frequency	11 kV, 50 Hz
Grid Impedance	4 Ω, 60 mH
DC Link Voltage	3.5 kV
DC Link Capacitance	1000 µF
Inductances (L_G, L_1 and L_2)	30 mH, 25 mH and 15 mH
Filter resistance and capacitance (R_f and C_f)	2 Ω and 100 mH
PV Array	**460kW**
Parallel Strings	20
Series connected modules per string	100
Open Circuit Voltage	37
Short Circuit Current	8.4
Voltage at Maximum Power Point	30
Current at Maximum Power Point	7.67
PMSG	**300kW**

Case-1: Change in Load

If the microgrid's load, demands more power than PVGS and WGS generation capacity, remaining power is drawn from the grid via back to back converters. In the control strategy of back to back converters, an initial reference active power of 0.5 MW is employed and then decreased to 0.25 MW between 0.1 and 0.3 seconds. The reactive power reference is set at 1 MVAr. The active and reactive powers of the connected dynamic load initially decrease from 1 MW and 2 MVAr to 0.25 MW and 0.5 MVAr at 0.1 second. Subsequently, they are reduced to 0.5 MW and 1 MVAr at 0.3 seconds, further reduced to 0.75 MW and 1.5 MVAr at 0.6 seconds, and

finally raised to 1 MW and 2 MVAr at 0.85 seconds. The control strategy effectively ensures the tracking of the reference active and reactive power input by comparing it to the actual active and reactive power injected into the grid, as illustrated in Figure 9. PVGS and WGS provide the extra active and reactive powers required for the dynamic load, as shown in Figure 9. The grid quickly aligns with the reference active and reactive power, achieving stabilization within three fundamental cycles. The tracking error under steady-state conditions remains below 0.15%, accompanied by a peak overshoot of 0.25%. The DC link voltage of the back to back converter closely follows the reference voltage of 3.5 kV, as depicted in Figure 10.When there are variations in the grid-injected power, the DC link voltage undergoes fluctuations around its reference value but quickly converges and tracks it within a span of 4 fundamental cycles. The controller angle is visually represented in the figure 10.

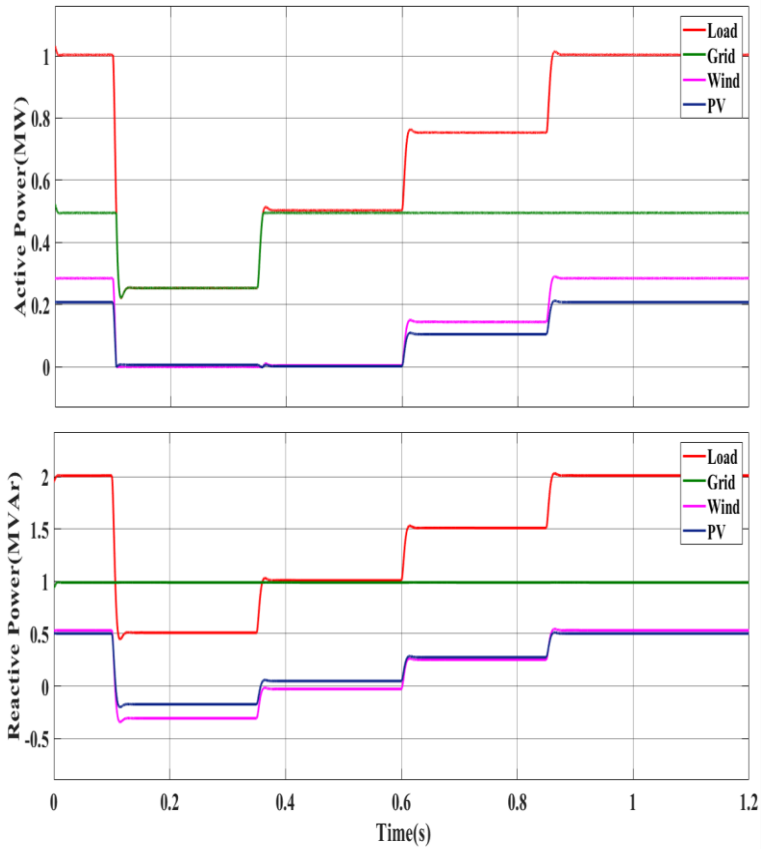

Figure 9. Active and reactive power sharing among Grid, Wind and PV generation system for load change

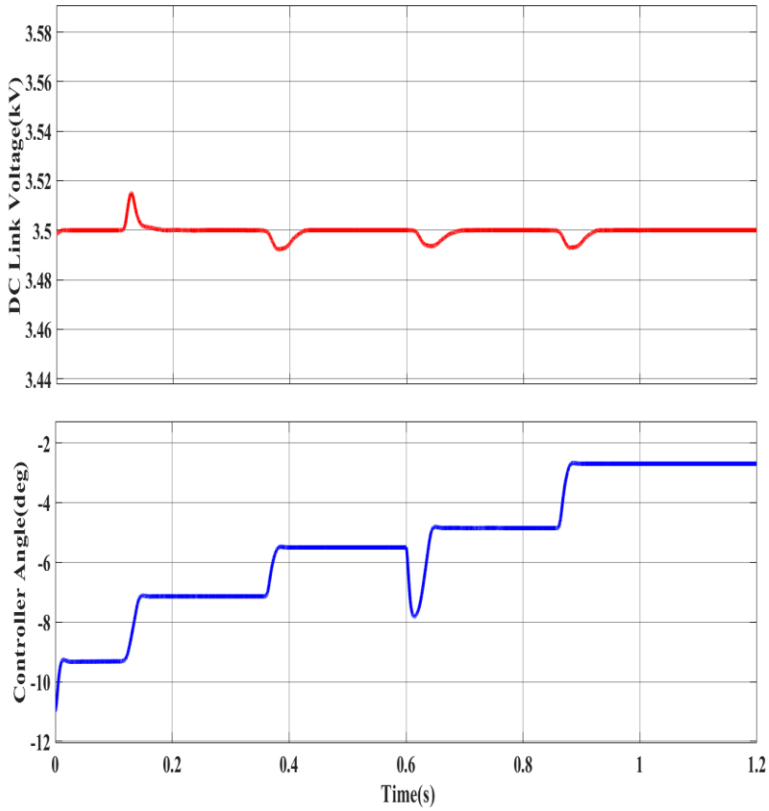

Figure 10. DC link voltage of back to back converter and controller angle

Case-2: Increase in Load

The reference active power starts at 0.5 MW and increases to 1 MW over a period of 0.6 to 0.85 seconds. The reference reactive power is set at 1 MVAr at the same time. The active and reactive powers of the connected dynamic load changed from 1 MW and 2 MVAr to 1.25 MW and 2.5 MVAr at 0.1 second. And then altered to 1.5 MW and 3 MVAr at 0.3 seconds, further to 2 MW and 4 MVAr at 0.6 seconds and finally to 1 MW and 2 MVAr at 0.85 seconds. The control strategy exhibits effective tracking, with the reference active power input aligning closely with the actual grid-injected active power, as depicted in the figure 11. Similarly, the grid adeptly tracks the reference reactive power. The renewable energy sources PVGS and WGS fulfil the remaining active and reactive power needs of the dynamic load.

The transient response of the grid's tracking of reference active and reactive power is less than two fundamental cycles and achieved a steady state within three fundamental cycles. The tracking error during steady-state conditions is less than 0.12%, and a peak overshoot of 0.2%. Figure 11 illustrates the sharing of active and reactive power among the Grid, Wind,

and PV generation systems during changes in load. Additionally, Figure 12 shows the efficient tracking of the DC link voltage of the back to back converter to the reference voltage of 3.5kV. When encountering variations in grid-injected power, the DC link voltage exhibits momentary fluctuations around its reference value, promptly converging and tracking within a span of four fundamental cycles. The controller angle is visually represented in the accompanying figure 12. Load current, grid current, PVGS current and WGS current are presented in figure 13. Grid current and voltage THD are presented in figure 14.

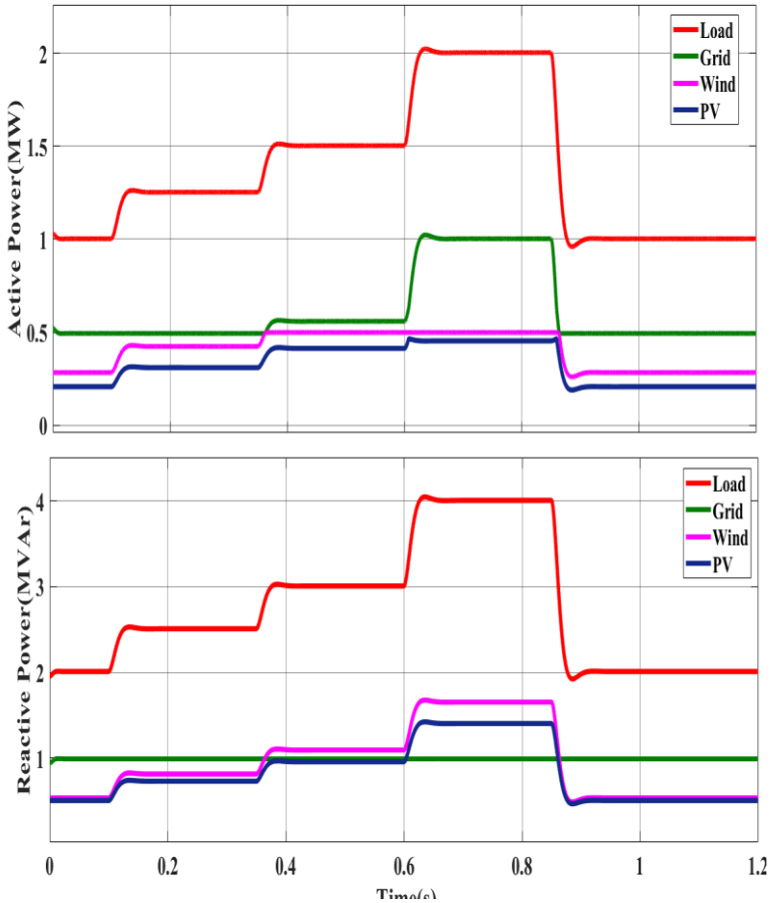

Figure 11. Active and reactive power sharing among Grid, Wind and PV generation system for load increase

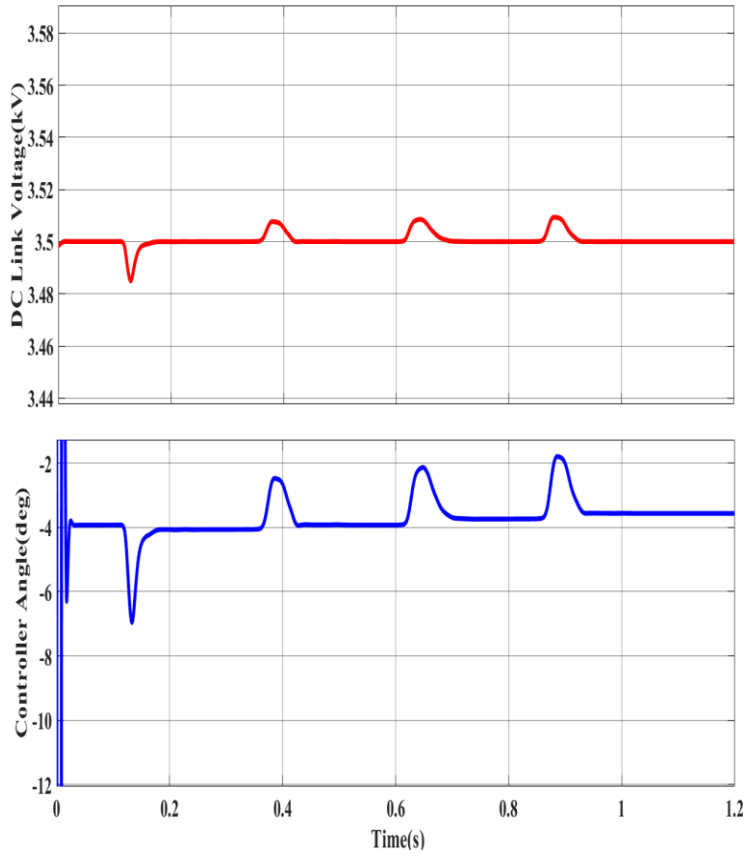

Figure 12. DC link voltage of back to back converter and controller angle during load increase

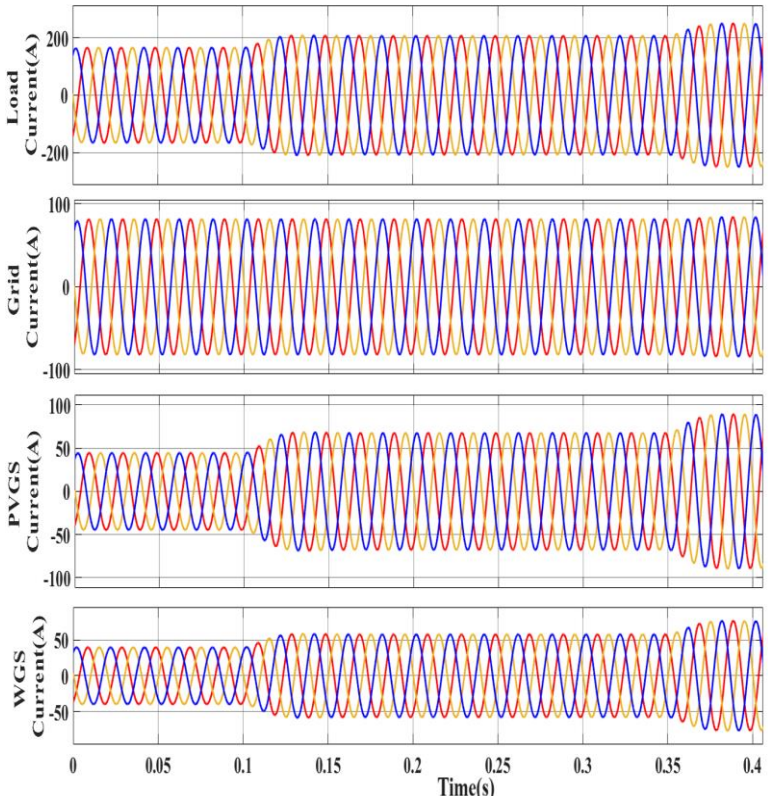

Figure 13. Currents during load increase

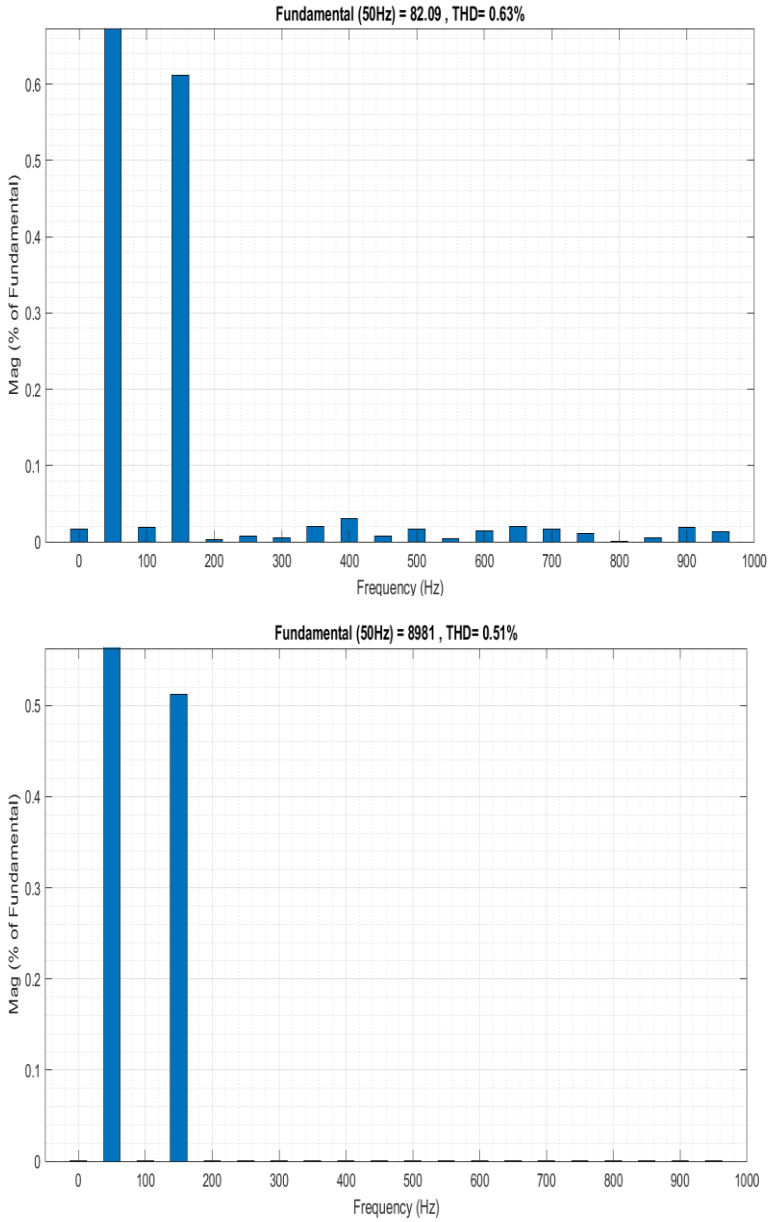

Figure 14. Grid current and voltage THD

Case-3: Change in frequency

Adopting a back to back converter can provide isolation between the grid and the renewable sources during frequency and voltage disturbances. Figure 15 depicts response of real and imaginary powers to a frequency instability on the grid side, occurring between 0.05 seconds and 0.25 seconds. At the start of 0.05 seconds, the grid frequency reduced by 0.5% and at 0.25 seconds it returned to system's fundamental value of 50Hz. The system's response shows that, despite fluctuations in the real and imaginary power injections from the grid to VSC-1, both the injected and load power into the microgrid remain constant. This emphasizes the back to back converter connection's ability to insulate the microgrid from

disruptions in the utility's frequency, ensuring stability and a consistent power supply to the microgrid throughout the observed period.

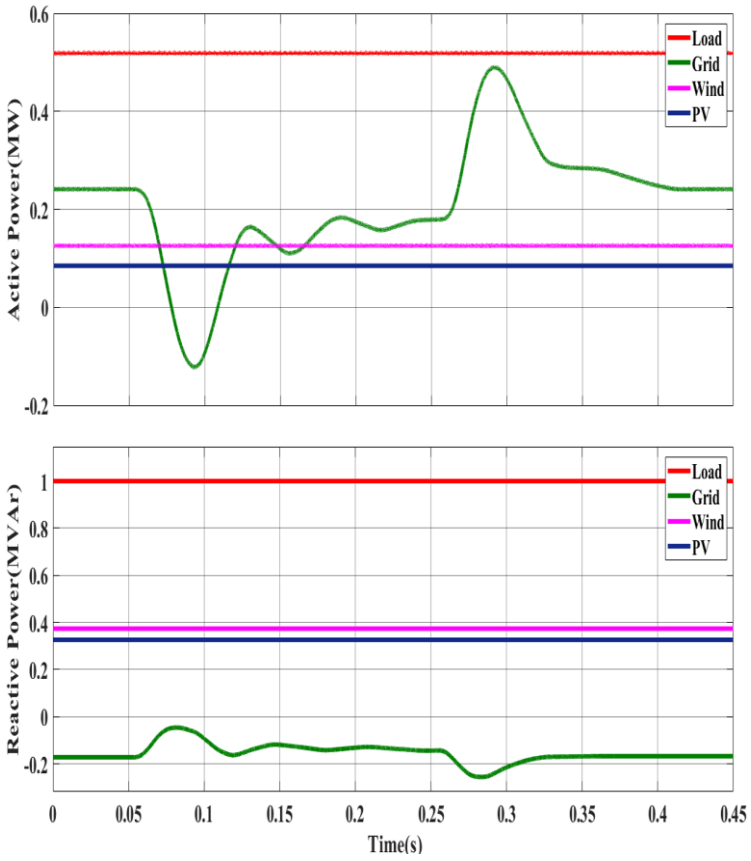

Figure 15. Active and reactive power sharing among Grid, Wind and PV generation system for frequency variation

Case-4: Voltage Sag

In steady-state conditions, a partial voltage imbalance in the grid voltage happens at 0.1 seconds and is rectified after 0.5 seconds. Figure 16 shows the power and reactive power profiles during this incidence. Notably, the load power and the injected power into the microgrid exhibit minimal disturbance. The real power drawn from the grid, despite transient variations at the onset and conclusion of the sag, remains consistent at the steady-state level to uphold power supply to the microgrid. At the same time, the imaginary power changes from positive to negative due to the voltage drop in the utility, making it to absorb reactive power. Throughout this disturbance, the DC capacitor assists the utility by supplying reactive power.

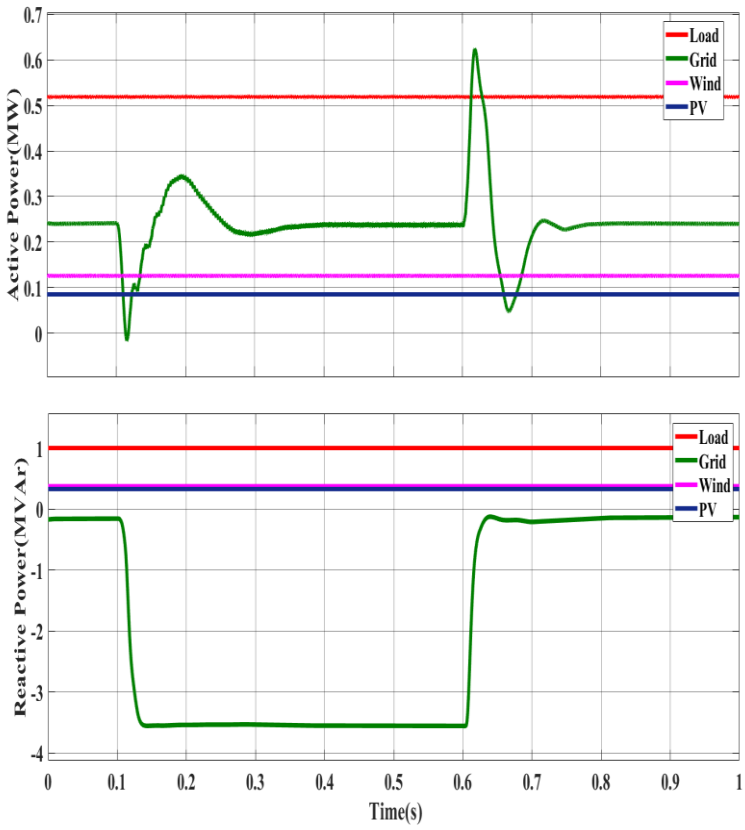

Figure 16. Active and reactive power sharing among Grid, Wind and PV generation system for Voltage sag

7. Conclusion

This research highlights the critical importance of robust power management and control mechanisms in utility-connected microgrids incorporating solar and wind energy sources. Using back to back converters is essential for precisely controlling the transfer of both real and imaginary power among the microgrid and utility. The suggested control strategy operates in two distinct states for efficiently distributing power exchange. In State-1, a reference of both real and imaginary power is distributed among the microgrid and the utility through back to back converters. State-2 is the stage at which the DGs in the microgrid reach their peak threshold power, necessitating the utility to meet the remaining power demand. Coordination among DGs ensures seamless load balancing in both ISM and GCM modes. Importantly, the back to back converters play an important role in frequency isolation, protecting the microgrid from frequency and voltage variations on the grid side. Implementing coordinated relay-breaker operation during faults, along with blocking the back to back converters, ensures a smooth reintegration after fault clearance. System

stability is thoroughly validated under diverse load variations, and the proposed control arrangement demonstrates resilience to fluctuations in grid-side voltage and frequency. This robustness guarantees continuous and dependable power sharing across varied operating conditions. Simulation results performed in MATLAB/SIMULINK affirm the efficacy of the control strategy, show its potential to enhance the constancy and reliability of grid-connected microgrids incorporating solar and wind energy sources. This research contributes significantly to the advancement of sustainable energy solutions, offering a robust and environmentally friendly approach to power systems. By addressing challenges and proposing innovative solutions, it paves the way for the continued development and integration of renewable energy sources, ultimately fostering resilient and sustainable power infrastructures.

References

1. Kornbluth, Yosef, Gabriel Cwilich, Sergey V. Buldyrev, Saleh Soltan, and Gil Zussman. "Distribution of blackouts in the power grid and the Motter and Lai model." Physical Review E 103, no. 3 (2021): 032309.
2. Priyadarshini, I., Mohanty, P., Kumar, R., Son, L.H., Chau, H.T.M., Nhu, V.H., Thi Ngo, P.T. and Tien Bui, D., 2020, May. Analysis of outbreak and global impacts of the COVID-19. In Healthcare (Vol. 8, No. 2, p. 148). MDPI.
3. Vargas, R., Macedo, L.H., Home-Ortiz, J.M., Mantovani, J.R.S. and Romero, R., 2021. Optimal restoration of active distribution systems with voltage control and closed-loop operation. IEEE Transactions on Smart Grid, 12(3), pp.2295-2306.
4. Shen, W., Chen, X., Qiu, J., Hayward, J.A., Sayeef, S., Osman, P., Meng, K. and Dong, Z.Y., 2020. A comprehensive review of variable renewable energy levelized cost of electricity. Renewable and Sustainable Energy Reviews, 133, p.110301.
5. Violante, W., Canizares, C.A., Trovato, M.A. and Forte, G., 2020. An energy management system for isolated microgrids with thermal energy resources. IEEE Transactions on Smart Grid, 11(4), pp.2880-2891.
6. Singh, J., Prakash Singh, S., Shanker Verma, K., Iqbal, A. and Kumar, B., 2021. Recent control techniques and management of AC microgrids: A critical review on issues, strategies, and future trends. International Transactions on Electrical Energy Systems, 31(11), p.e13035.
7. Vuddanti, S. and Salkuti, S.R., 2021. Review of energy management system approaches in microgrids. Energies, 14(17), p.5459.

8. Salehi, N., Martínez-García, H., Velasco-Quesada, G. and Guerrero, J.M., 2022. A comprehensive review of control strategies and optimization methods for individual and community microgrids. IEEE access, 10, pp.15935-15955.
9. Solanke, T.U., Khatua, P.K., Ramachandaramurthy, V.K., Yong, J.Y. and Tan, K.M., 2021. Control and management of a multilevel electric vehicle's infrastructure integrated with distributed resources: A comprehensive review. Renewable and Sustainable Energy Reviews, 144, p.111020.
10. Espín-Sarzosa, D., Palma-Behnke, R. and Núñez-Mata, O., 2020. Energy management systems for microgrids: Main existing trends in centralized control architectures. Energies, 13(3), p.547.
11. Gulzar, Muhammad Majid, Ayesha Iqbal, Daud Sibtain, and Muhammad Khalid. "An innovative converterless solar PV control strategy for a grid connected hybrid PV/wind/fuel-cell system coupled with battery energy storage." IEEE Access 11 (2023): 23245-23259.
12. Lu, Xi, Shiwei Xia, Guangzeng Sun, Junjie Hu, Weiwei Zou, Quan Zhou, Mohammad Shahidehpour, and Ka Wing Chan. "Hierarchical distributed control approach for multiple on-site DERs coordinated operation in microgrid." International Journal of Electrical Power & Energy Systems 129 (2021): 106864.
13. Wang, D., Weyen, D. and Van Tichelen, P., 2023. Proposals for Updated EMC Standards and Requirements (9–500 kHz) for DC Microgrids and New Compliance Verification Methods. Electronics, 12(14), p.3122.
14. Mosayebi, M., Sadeghzadeh, S.M., Khooban, M.H. and Guerrero, J.M., 2020. Decentralised non-linear I–V droop control to improve current sharing and voltage restoration in DCNG clusters. IET Power Electronics, 13(2), pp.248-255.
15. Elgammal, Adel, and Tagore Ramlal. "Adaptive voltage regulation control strategy in a stand-alone islanded DC microgrid based on distributed wind/photovoltaic/diesel/energy storage hybrid energy conversion system." European Journal of Electrical Engineering and Computer Science 5, no. 4 (2021): 26-33.
16. Sivadasan, J., Vignesh, R., Antony Robinson, J., Justin Diraviam, J., Senthilkumar, S. and Aandal, R., 2023, May. A switched boost landsman converter with ANFIS based MPPT for grid connected wind energy system. In AIP Conference Proceedings (Vol. 2618, No. 1). AIP Publishing.
17. Cao, D., Zhao, J., Hu, W., Ding, F., Huang, Q. and Chen, Z., 2021. Attention enabled multi-agent DRL for decentralized volt-VAR control of active distribution system using PV inverters and SVCs. IEEE transactions on sustainable energy, 12(3), pp.1582-1592.

18. Li, D., Wu, Z., Zhao, B. and Zhang, L., 2020. An improved droop control for balancing state of charge of battery energy storage systems in AC microgrid. IEEE Access, 8, pp.71917-71929.
19. Pham, M.D. and Lee, H.H., 2020. Effective coordinated virtual impedance control for accurate power sharing in islanded microgrid. IEEE Transactions on Industrial Electronics, 68(3), pp.2279-2288.
20. Li, X., Shang, Z., Peng, F., Li, L., Zhao, Y. and Liu, Z., 2021. Increment-oriented online power distribution strategy for multi-stack proton exchange membrane fuel cell systems aimed at collaborative performance enhancement. Journal of Power Sources, 512, p.230512.
21. Jiang, E., Zhao, J., Shi, Z., Mi, Y., Lin, S. and Muyeen, S.M., 2023. Intelligent Virtual Impedance Based Control to Enhance the Stability of Islanded Microgrid. Journal of Electrical Engineering & Technology, 18(5), pp.3971-3984.
22. Pham, X.H.T., 2020. Power sharing strategy in islanded microgrids using improved droop control. Electric Power Systems Research, 180, p.106164.